

WALL-TEMPERATURE AND UNDERWEDGE-SURFACE ANGLE INFLUENCE ON THE FLOWFIELD STRUCTURE OF A SHARP LEADING EDGE IN HYPERSONIC FLOW

Wilson F. N. Santos, Wilson@lcp.inpe.br

Combustion and Propulsion Laboratory
National Institute for space Research
Cachoeira Paulista, SP 12630-000

Abstract. Hypersonic flow past sharp leading edges at zero incidence is investigated for a range of body-surface temperature from 440 to 1760 K. The simulations were performed by using the Direct Simulation Monte Carlo (DSMC) method. Distributions of the primary properties ahead of the sharp leading edges for five different underwedge-surface angles are compared in order to assess the relative importance of the underwedge-surface angle and the wall temperature to the upstream disturbance. The results highlighted some significant differences on the flowfield properties due to variations on the underwedge-surface angle and on the wall temperature. It was found that the upstream effects have different influence on velocity, density, pressure and temperature along the stagnation streamline ahead of the leading edges. Interesting features observed in the flowfield structure showed that small underwedge-surface angle has important effects on high Mach number leading edge flows.

Keywords: Hypersonic Flow, Rarefied Flow, DSMC, Sharp Leading Edge, Underwedge-surface angle.

1. INTRODUCTION

The problem of hypersonic low density flow over flat plates and wedges aligned with the flow has been extensively investigated experimentally and theoretically. Experimental and theoretical works on these shapes have been concentrated primarily on the analysis of the flowfield structure by considering the leading edges as being aerodynamically-sharp, and with a finite bevel angle in the case of plates. The reason for that is because all the experimental work has suffered with the problem of assessing the influence of the tip thickness t and underwedge angle θ (see Fig. 1) on the measurements of the flowfield properties on the flat-plate surface, since it is not possible to investigate experimentally the special case of zero-tip thickness with or without zero-degree underwedge-surface angle. Physically, some of the molecules that collide with the frontal face, with the underwedge surface or on the top of the flat plate are emitted in an upstream direction. These reflected molecules collide with the incoming freestream molecules, thereby altering the flow about the idealized flat plate or sharp-edged wedge. Furthermore, experimental difficulty arises from the complication of installing pressure taps very close to the nose of the leading edge. In low-density flows, the true pressure on a surface can be significantly different from that measured in orifice cavities or pressure holes, because of the increase in the effect of molecule-surface collisions, the so-called orifice effect (Potter et al., 1966).

A critical study providing information on maximum allowable tip thickness or underwedge-surface angle for a given flow pattern has not received considerable attention. Such information is important when a comparison is to be made between experimental results in the immediate vicinity of the leading edge and the theoretical results, which generally assume a zero-thickness leading edge.

In this scenario, Santos (2001) has investigated the sensitivity of the flowfield structure and the aerodynamic surface quantities to leading-edge thickness variations for a flat plate in a low-density hypersonic flow. The range of Knudsen number, based on the tip thickness t , covered from the transition flow regime to the free molecular flow regime. Nevertheless, the effect of the underwedge-surface angle θ was not investigated, since it was assumed zero-degree angle.

Santos (2007) has investigated closer the underwedge-surface angle effects. A parametric study was performed on a flat plate in order to assess the impact on the primary properties upstream the nose of the leading edge and on the aerodynamic surface quantities due to variations on the underwedge-surface angle with zero-tip thickness. The simulations pointed out that the aerodynamic surface quantities increased on the upper surface of the flat plate with the underwedge-surface angle rise. It was found that pressure was more affected than the heat flux with increasing the underwedge-surface angle.

In an effort to obtain further insight into the nature of the flowfield structure of sharp leading edge under hypersonic transition flow conditions, the primary interest in the present account is to extend further the previous analysis (Santos, 2001 and 2007) by investigating the impact of the wall temperature along with the underwedge-surface angle effects.

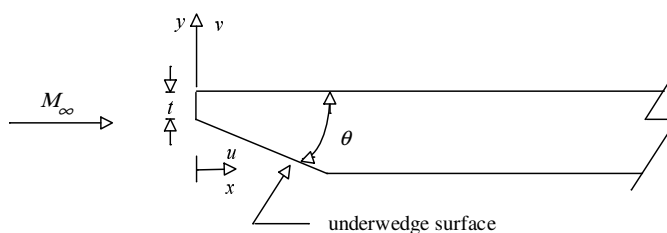


Figure 1: Drawing illustrating the leading edge shape.

2. COMPUTATIONAL METHOD AND PROCEDURE

The most successful numerical technique for modeling complex transitional flows has been the Direct Simulation Monte Carlo (DSMC) method (Bird, 1994). The DSMC method simulates real gas flows with various physical processes by means of a huge number of modeling particles; each particle represents a fixed number of real gas molecules. In the DSMC model, the particle evolution is divided into two independent phases during the simulation; the movement phase and the collision phase. In the movement phase, all particles are moved over distances appropriate to a short time interval, time step, and some of them interact with the domain boundaries in this time interval. Particles that strike the solid wall would reflect according to the appropriate gas-surface interaction model, specular, diffusive or a combination of these. In the collision phase, intermolecular collisions are performed according to the theory of probability without time being consumed. In this context, the intermolecular collisions are uncoupled to the translational molecular motion over the time step used to advance the simulation. Time is advanced in discrete steps such that each step is small in comparison with the mean collision time. The simulation is always calculated as unsteady flow. However, a steady flow solution is obtained as the large time state of the simulation.

Collisions in the present DSMC code are modeled by using the variable hard sphere (VHS) molecular model (Bird, 1981) and the no time counter (NTC) collision sampling technique (Bird, 1994). Repartition energy among internal and translational modes is controlled by the Borgnakke-Larsen statistical model (Borgnakke and Larsen, 1975). Simulations are performed using a non-reacting gas model consisting of N_2 and O_2 . Energy exchanges between the translation and internal modes, rotation and vibration, are considered. Relaxation collision numbers of 5 and 50 were used for the calculations of rotation and vibration, respectively.

For the numerical treatment of the problem, the flowfield around the leading edge is divided into an arbitrary number of regions, which are subdivided into computational cells. Cells are further subdivided into subcells, two subcells/cell in each coordinate direction. The cell provides a convenient reference for the sampling of the macroscopic gas properties, while the collision partners are selected from the same subcell for the establishment of the collision rate. The computational domain used for the calculation is made large enough so that body disturbances do not reach the upstream and side boundaries, where freestream conditions are specified.

3. COMPUTATIONAL CONDITIONS

The freestream and flow conditions used in the present calculations are those given by Santos (2007) and summarized in Table 1. The gas properties (Bird, 1994) employed in the simulations are shown in Table 2.

Table 1: Freestream Conditions

Temperature T_∞ (K)	Pressure p_∞ (N/m ²)	Density ρ_∞ (kg/m ³)	Number density n_∞ (m ⁻³)	Viscosity μ_∞ (Ns/m ²)	Mean free path λ_∞ (m)	Velocity V_∞ (m/s)
220.0	5.582	8.753×10^{-5}	1.8209×10^{21}	1.455×10^{-5}	9.03×10^{-4}	3560

Table 2: Gas Properties

	Mole fraction X	Molecular mass m (kg)	Molecular diameter d (m)	Viscosity index ω
O_2	0.237	5.312×10^{-26}	4.01×10^{-10}	0.77
N_2	0.763	4.65×10^{-26}	4.11×10^{-10}	0.74

The freestream velocity U_∞ , assumed to be a constant at 3.56 km/s, corresponds to freestream Mach number M_∞ of 12. The translational and vibrational temperatures in the freestream are in equilibrium at 220 K.

In the previous study, Santos (2001), the reference flow scale was defined as being the tip thickness t of the flat plate. The tip thickness investigated was t/λ_∞ of 0.2, 0.1, 0.05, 0.025, 0.02, 0.0125 and 0.01, where λ_∞ was the freestream mean free path. Therefore, the overall Knudsen number Kn_t , defined as the ratio of the freestream mean free path λ_∞ to the tip thickness t , corresponded to 5, 10, 20, 40, 50, 80 and 100, respectively.

In the present account, in order to simulate the underwedge-angle effects the DSMC calculations were performed independently for five distinct numerical values of underwedge-surface angle θ of 5, 10, 15, 20 and 25 degrees with zero-thickness flat plate, which represents Kn_t of infinity.

In order to simulate the wall temperature effect, the DSMC calculations were performed independently for three distinct numerical values of wall temperature, i.e., T_w of 440 K, 880 K and 1760 K. These values correspond to 2, 4 and 8 times the freestream temperature, respectively.

Finally, the Reynolds number per unit of meter is $Re_\infty = 21416.3$, also based on conditions in the undisturbed stream.

It should be emphasized that, computational investigation presents advantages on experimental investigation in the sense that leading edge with zero-tip thickness is only possible in a computational study.

4. COMPUTATIONAL RESULTS AND DISCUSSION

The tangential velocity profiles upstream the leading edge and their dependence on the underwedge-surface angle θ and on the wall temperature T_w are illustrated in Figs. 2 and 3 for wall temperature of 440 K and 1760 K, respectively. In this set of plots, the velocity ratio represents the tangential velocity u normalized by the freestream velocity U_∞ , the dimensionless height stands for the height y , normal to the stagnation line of the leading edge, normalized by the freestream mean free path λ_∞ , and X represents the upstream length x along the stagnation line of the leading edge also normalized by λ_∞ .

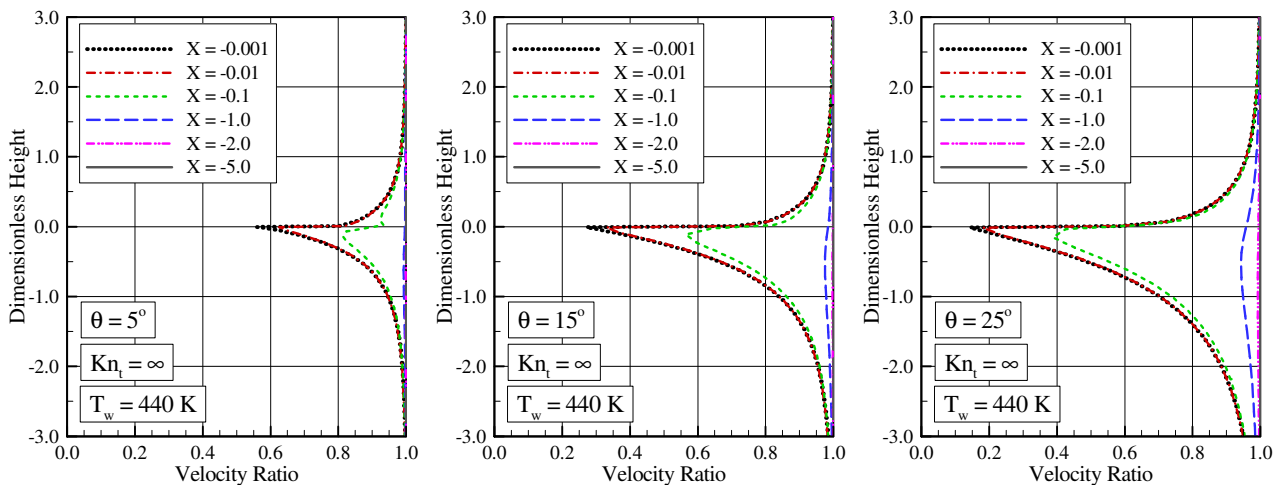


Figure 2: Tangential velocity (u/U_∞) profiles upstream of the leading edge for underwedge-surface angle θ of (a) 5, (b) 15, and (c) 25 degrees and wall temperature of 440 K.

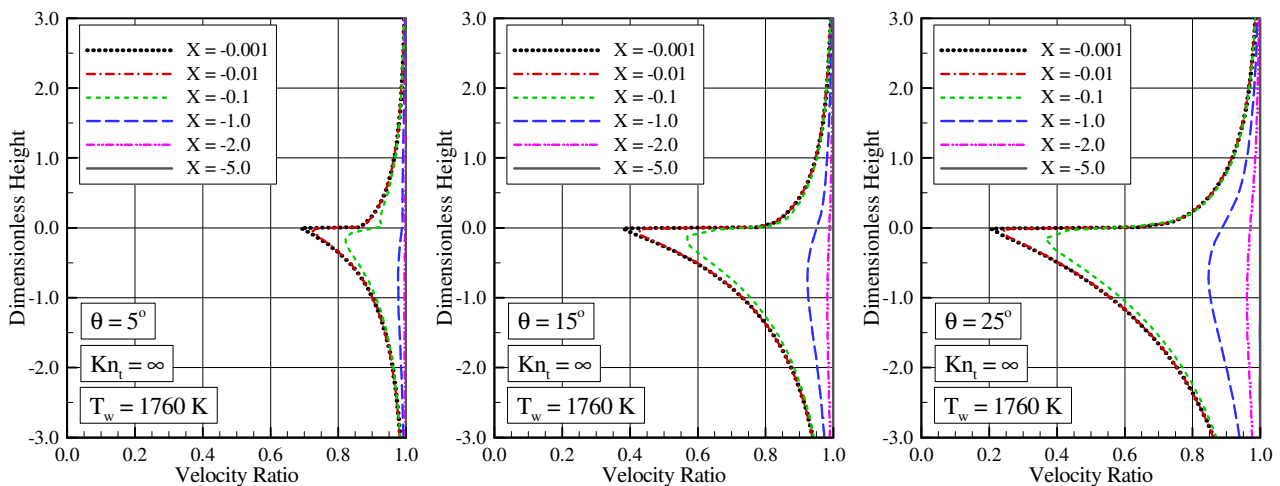


Figure 3: Tangential velocity (u/U_∞) profiles upstream of the leading edge for underwedge-surface angle θ of (a) 5, (b) 15, and (c) 25 degrees and wall temperature of 1760 K.

According to Figs. 2(a-c), it is clearly noted that, even for the $\theta = 5^\circ$ case, the velocity profiles are asymmetric about the centerline, $y/\lambda_\infty = 0$, and has a relative minimum value along the centerline. As the underwedge-surface angle increases, the profiles become much more asymmetric and the minimum value on the profiles occurs below the centerline. This behavior indicates that the contribution to the asymmetry in the upstream disturbance arises due to the underwedge-surface angle as would be expected. It is also noted that, for the 5-degree underwedge-surface angle, the velocity profile at station $X = -1.0$ is not affected anymore for the presence of the lower surface. In contrast, for the other two cases shown, underwedge-surface angle θ of 15 and 25 degrees, the lower surface still affects the velocity profiles more upstream of the leading edge nose. Of particular interest is the behavior of the velocity ratio at the vicinity

of the leading-edge nose, at station $X = -0.001$. For the 5-degree underwedge-surface angle case, the tangential velocity is still 55% of the freestream velocity U_∞ . Nevertheless, for the 25-degree underwedge-surface angle case, the tangential velocity is reduced to around 15% of U_∞ . It should also be mentioned in this context that as the underwedge-surface angle increases the leading edge becomes blunt for the freestream molecules.

Referring to Figs. 3(a-c), it is seen that the tangential velocity profiles are affected by the wall-temperature rise. As a result, the upstream disturbance increases by increasing the wall temperature. For instance, it is observed that, for the wall-temperature case of 440 K, the velocity profiles at station $X = -2.0$ are not affected anymore by the presence of the lower surface. Conversely, for the wall-temperature case of 1760 K, the lower surface still affects the velocity profiles more upstream of the leading edge nose.

Density profiles at six locations upstream the leading edges are plotted in Figs. 4 and 5 for wall temperature of 440 K and 1760 K, respectively, and parameterized by the underwedge-surface angle θ . In this set of plots, density ratio stands for density ρ normalized by the freestream density ρ_∞ .

According to Figs. 4(a-c), it is seen that density profiles follow the same trend of those for velocity profiles in the sense that they are clearly asymmetric with respect to the centerline. For the 5-degree underwedge-surface angle case, the pick value for density ρ , at station $X = -0.001$, takes place at the vicinity of the centerline and it is around 1.5 times the freestream density ρ_∞ . For the 25-degree underwedge-surface angle case, the pick value increases to approximately 5.0 times the freestream density ρ_∞ . For comparison purpose, for 10- and 20-degree underwedge-surface angles, the density ratio (not shown) is around 2.4 and 4.2, respectively. By comparing these values, one can see that the upstream disturbance along the centerline does not double when the underwedge-surface angle doubles.

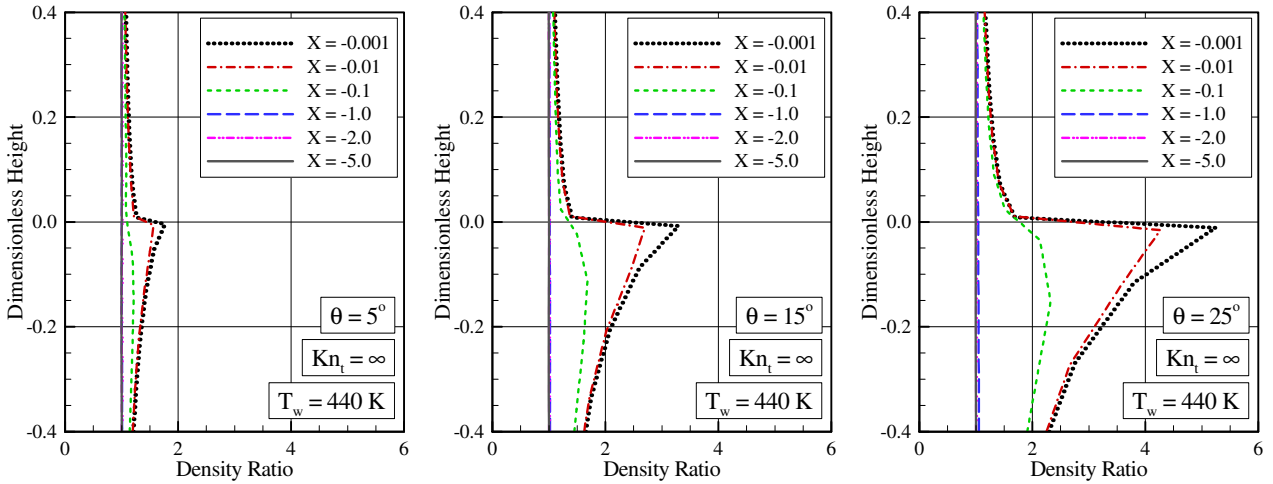


Figure 4: Density (ρ/ρ_∞) profiles upstream of the leading edge for underwedge-surface angle θ of (a) 5, (b) 15, and (c) 25 degrees and wall temperature of 440 K.

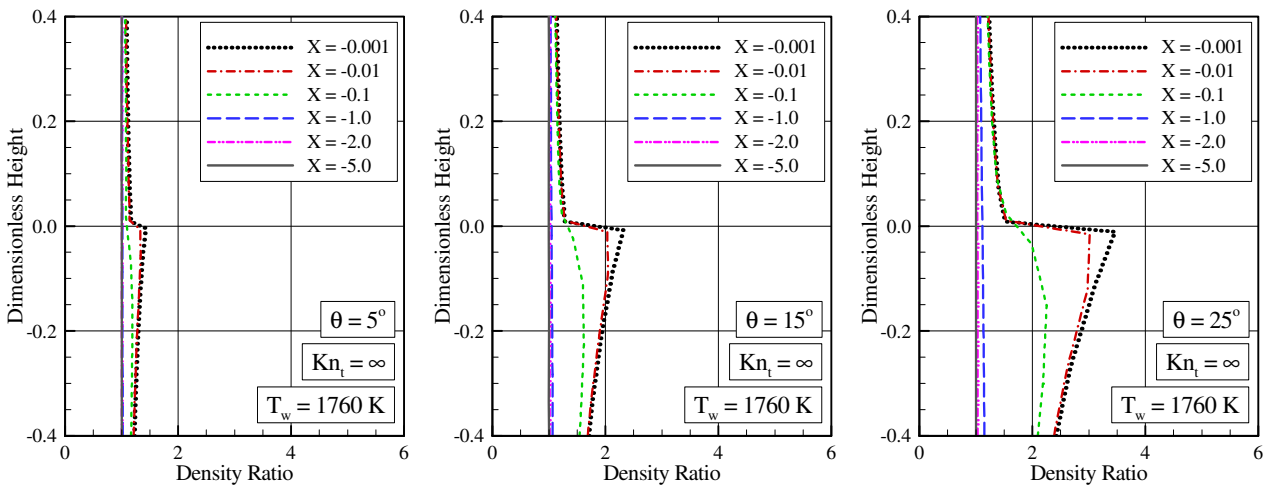


Figure 5: Density (ρ/ρ_∞) profiles upstream of the leading edge for underwedge-surface angle θ of (a) 5, (b) 15, and (c) 25 degrees and wall temperature of 1760 K.

Another flow peculiarity is observed as the plots in Fig. 4 are compared to those in Fig. 5. Near the stagnation point, $X = -0.001$, a substantial density increase occurs with decreasing wall temperature T_w . This is a characteristic of cold-wall flow. In this type of flow, the body surface temperature is low compared to the stagnation temperature. This leads to a steep density gradient near the body surface. For the present simulation, the ratio of wall temperature to stagnation temperature changes from 0.07 to 0.27, which correspond to a cold-wall flow.

Pressure profiles upstream the leading edges are displayed as a function of the underwedge-surface angle θ in Figs. 6 and 7 for wall temperature of 440 K and 1760 K, respectively. In these figures, pressure p is normalized by the freestream pressure p_∞ . It is observed that the underwedge-angle effects on pressure profiles are similar to those observed in the density profiles in the sense that it increases with increasing the underwedge-surface angle. At the vicinity of the leading edge nose, at station $X = -0.001$, the pick value for pressure p takes place along the centerline and is around 30 times the freestream pressure p_∞ for the 5-degree underwedge-angle case, as shown in Fig. 6(a). For the 25-degree underwedge-surface angle, the pick value increases to approximately 75 times the freestream pressure p_∞ , as displayed in Fig. 6(c).

According to these figures, it is seen that the underwedge-surface angle as well as the wall temperature influences the flowfield far upstream. This domain of influence increases with increasing both the underwedge-surface angle and the wall temperature. The underwedge-surface effect results from the upstream diffusion of particles that are reflected from the lower surface of the leading edge. Consequently, blunting the leading edge (by increasing θ) leads to significantly larger disturbance upstream of the body. In addition, the wall-temperature effect results from particles reflecting from hotter surface with greater energies that diffuse further upstream.

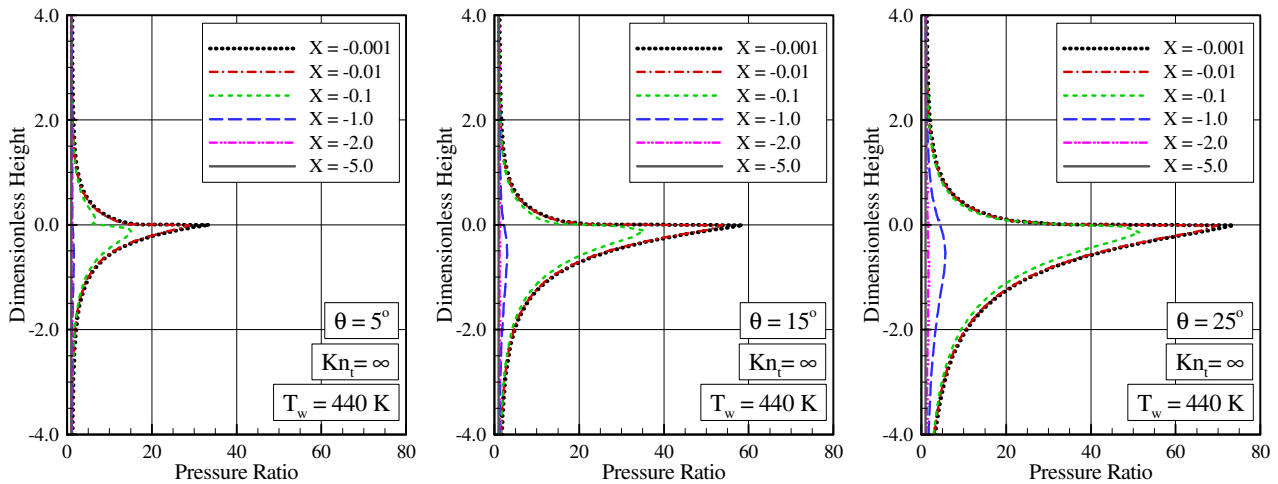


Figure 6: Pressure (p/p_∞) profiles upstream of the leading edge for underwedge-surface angle θ of (a) 5, (b) 15, and (c) 25 degrees and wall temperature of 440 K.

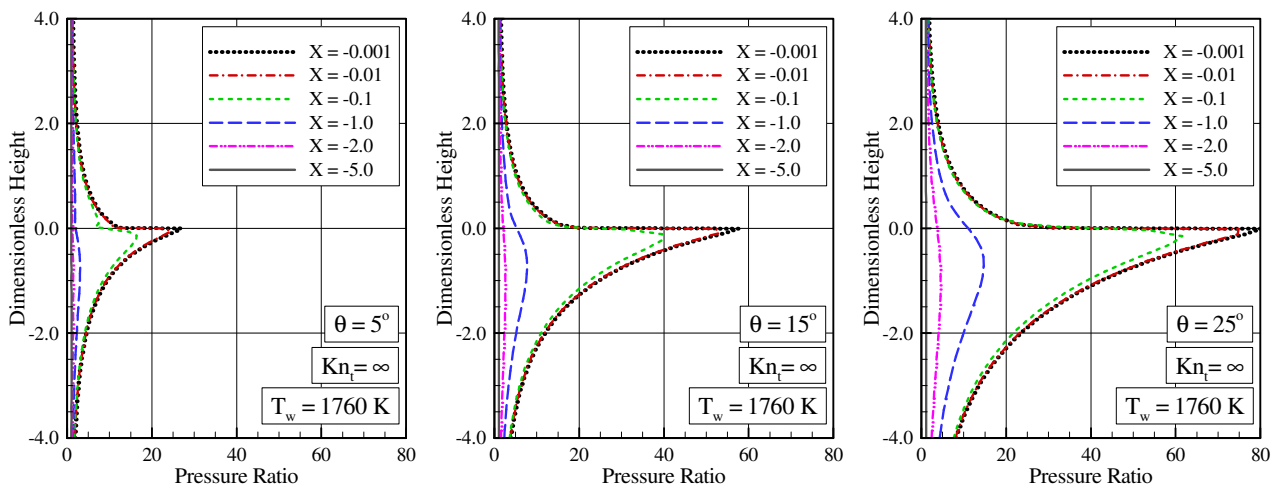


Figure 7: Pressure (p/p_∞) profiles upstream of the leading edge for underwedge-surface angle θ of (a) 5, (b) 15, and (c) 25 degrees and wall temperature of 1760 K.

It should be remarked that the upstream disturbance is more pronounced for pressure than that for density. As an illustrative example, for the 25-degree underwedge-angle case with wall temperature of 1760 K, pressure profile at station $X = -2.0$ is still affected by the underwedge-surface angle, Fig. 7(c). Conversely, for the same station, no disturbance is observed in the density profiles, Fig. 5(c).

Kinetic temperature profiles along the stagnation streamline are demonstrated in Fig. 8 as a function of the wall temperature T_w . In this figure, temperature ratio accounts for translational temperature T_T , rotational temperature T_R , vibrational temperature T_V and the overall temperature T_{OV} normalized by the freestream temperature T_∞ . Also, dimensionless length is the length x along the stagnation streamline normalized by the freestream mean free path λ_∞ . In addition, flow direction is from left to right hand side.

It is apparent from this figure that thermodynamic non-equilibrium occurs throughout the shock layer, as shown by the lack of equilibrium of the translational and internal kinetic temperatures. Thermal non-equilibrium occurs when the temperatures associated with the translational, rotational, and vibrational modes of a polyatomic gas are different. The overall kinetic temperature T_{OV} shown is defined for a non-equilibrium gas as the weighted mean of the translational and internal temperature (Bird, 1994) as follows,

$$T_{OV} = \frac{\xi_T T_T + \xi_R T_R + \xi_V T_V}{\xi_T + \xi_R + \xi_V} \quad (1)$$

where ξ_T , ξ_R , and ξ_V are the degrees of freedom associated to translational, rotational and vibrational energy modes, respectively.

The overall kinetic temperature T_{OV} is equivalent to the thermodynamic temperature only under thermal equilibrium conditions. As a matter of fact, it should be noticed that the ideal gas equation of state does not apply to this temperature in a non-equilibrium situation.

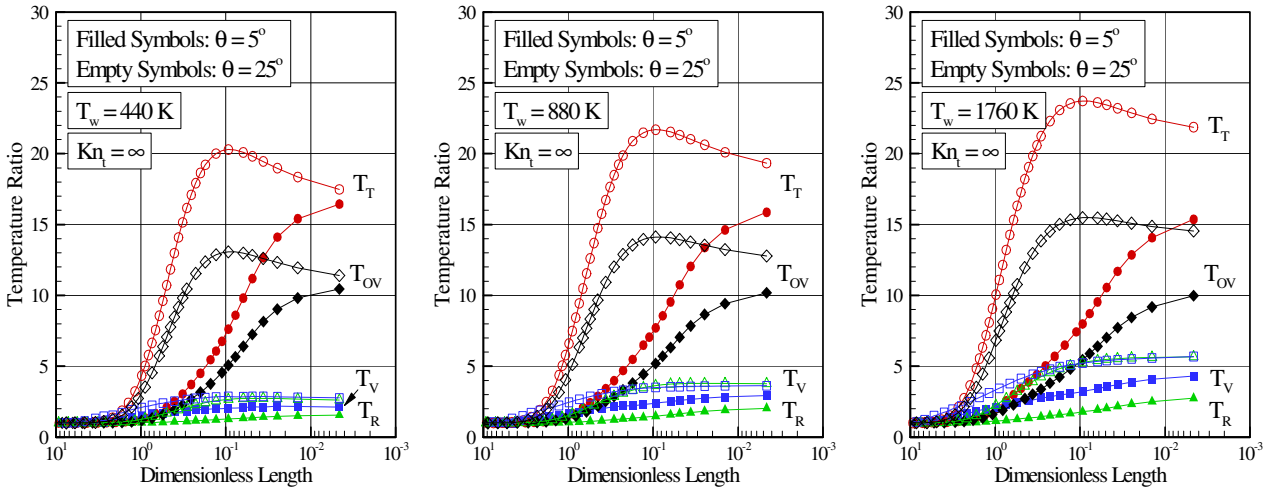


Figure 8: Kinetic temperature (T/T_∞) profiles upstream of the leading edges for wall temperature of (a) 440 K, (b) 880 K and (c) 1760 K.

Referring to Fig. 8, in the undisturbed freestream far from the leading edge, the translational and internal temperatures have the same value and are equal to the thermodynamic temperature. Approaching the nose of the leading edge, the translational temperature rises to well above the rotational and vibrational temperatures and reaches a maximum value that is a function of the underwedge surface angle. Still further downstream toward the nose of the leading edge, the translational temperature decreases and reaches a value on the wall that is above the wall temperature, resulting in a temperature jump as defined in continuum formulation.

Still referring to Fig. 8, it is firmly established that the underwedge-surface also angle affects the temperature profiles along the stagnation streamline. As the underwedge-surface angle is increased from 5 to 25 degrees, the leading edge becomes blunt. The translational kinetic temperature rise for blunt leading edges results from the essentially bimodal velocity distribution (Liepmann et al., 1964): the molecular sample consisting of mostly undisturbed freestream molecules with the molecules that have been reflected from the body surface. In this scenario, the translational kinetic temperature rise is a consequence of the large velocity separation between these two classes of molecules.

For the time being, it is instructive to explore the upstream disturbance effect on the overall kinetic temperature. In this way, overall temperature ratio profiles at six locations upstream the leading edges are demonstrated as a function of the underwedge-surface angle in Figs. 9 and 10 for wall temperature of 440 K and 1760 K, respectively. In this set of

plots, temperature ratio stands for the overall temperature T_{OV} normalized by the freestream temperature T_∞ .

Interesting features may be recognized from these set of diagrams. According to Fig. 9(a), it is seen that, for the 5-degree underwedge-surface angle, the maximum value for overall temperature, along the centerline, takes place at the vicinity of the stagnation point, at station $X = -0.001$. For 25-degree underwedge-surface angle, the maximum value for the overall temperature occurs around station $X = -0.1$. This is in agreement with the temperature profiles shown in Fig. 8. This behavior is explained by the fact that by increasing the underwedge-surface angle the leading edge becomes blunt. For blunt body, molecules reflecting basically from the lower surface collide with those oncoming freestream molecules, therefore high-velocity molecules. Consequently, the large velocity separation between these two classes of molecules results in a temperature rise far from the nose of leading edge as explained earlier.

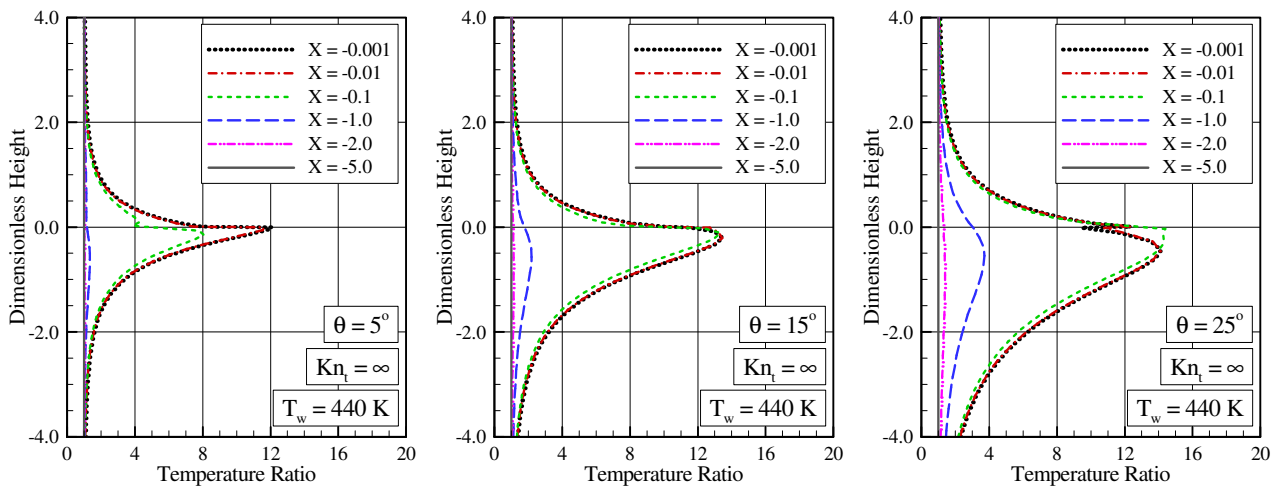


Figure 9: Overall temperature (T_{OV}/T_∞) profiles upstream of the leading edges for underwedge-surface angle θ of (a) 5, (b) 15, and (c) 25 degrees and wall temperature of 440 K.

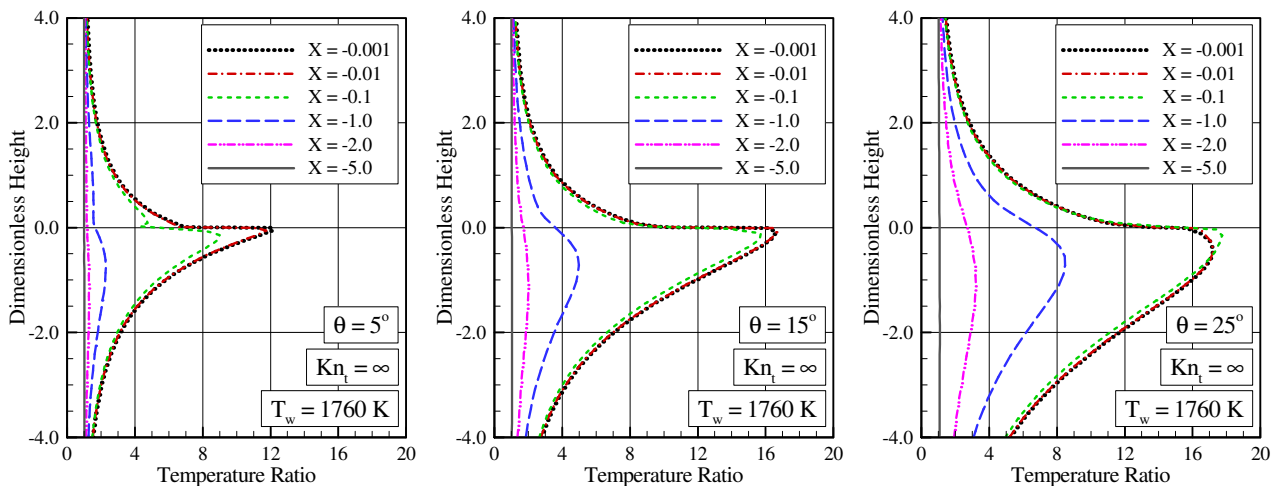


Figure 10: Overall temperature (T_{OV}/T_∞) profiles upstream of the leading edge for underwedge-surface angle θ of (a) 5, (b) 15, and (c) 25 degrees and wall temperature of 1760 K.

In an effort to provide additional information concerning the flowfield structure, dimensionless overall temperature contours, with streamlines patterns, on color maps, are illustrated in Fig. 11(a-c) for underwedge-surface angle of 5, 15 and 25 degrees, respectively, and wall temperature of 1760 K. In this group of plots, X and Y are the length x and height y , respectively, normalized by the freestream mean free path λ_∞ .

Referring to Figs. 11 (a-c), it is recognized that the streamlines along to and upper to the centerline are displaced upward by increasing the underwedge-surface angle θ . In addition to that, for the 15- and 25-degree underwedge-surface angle cases, the streamlines located immediately below to the centerline pass around the upper surface of the leading edge. A similar behavior is observed for the other wall temperature cases investigated. These results are extremely important in the sense that they indicate that, with the size of the models, for instance flat plate, being tested in hypersonic tunnels, significant effects on the flowfield properties as well as on the aerodynamic surface quantities,

due to leading-edge thickness and underwedge-surface angle, are possible even with models whose leading edges are generally considered as being either sharp or aerodynamically sharp.

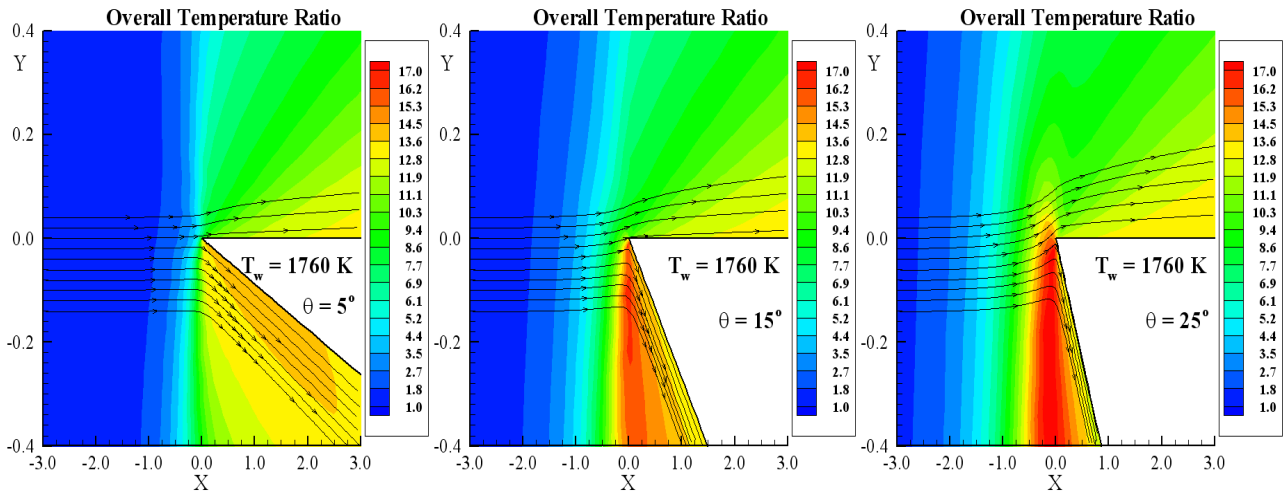


Figure 9: Overall temperature (T_{OY}/T_{∞}) contours at the vicinity of the leading edges for underwedge-surface angle θ of (a) 5, (b) 15, and (c) 25 degrees and wall temperature of 1760 K.

5. CONCLUDING REMARKS

This study applies the Direct Simulation Monte Carlo (DSMC) method to assess the impact on the flowfield structure due to variations on the underwedge-surface angle and on the surface temperature of flat plates. The calculations provided information concerning the upstream disturbance on the primary properties, such as velocity, density, pressure and temperature for the idealized situation of two-dimensional hypersonic rarefied flow.

The analysis showed that changes on the underwedge-surface angle disturbed the flowfield far upstream, as compared to the freestream mean free path. The domain of influence increased with increasing the underwedge-surface angle as well as with increasing the wall temperature of the flat plate. Moreover, the extent of the upstream flowfield disturbance is significantly different for each one of the primary properties. The domain of influence for temperature is larger than that observed for pressure and density.

Although this investigation has taken into account for a representative number of effects, a number of improvements to a realistic leading edge design is still desirable. The DSMC method has been used to assess the flowfield structure on flat plates by considering constant wall temperature. In a realistic design, temperature not only changes along the body surface but also inside the leading edge. In this scenario, a more detailed analysis that includes the conjugate heat transfer problem seems to be challenge.

7. REFERENCES

- Bird, G. A., 1981, "Monte Carlo Simulation in an Engineering Context", Progress in Astronautics and Aeronautics: Rarefied gas Dynamics, Ed. Sam S. Fisher, Vol. 74, part I, pp. 239-255, AIAA New York.
- Bird, G. A., 1994, "Molecular Gas Dynamics and the Direct Simulation of Gas Flows", Oxford University Press, Oxford, England, UK.
- Borgnakke, C. and Larsen, P. S., 1975, "Statistical Collision Model for Monte Carlo Simulation of Polyatomic Gas Mixture", Journal of Computational Physics, Vol. 18, n. 4, pp. 405-420.
- Liepmann, H. W., Narasimha, R. and Chahine, M., 1964, "Theoretical and Experimental Aspects of the Shock Structure Problem", Proceedings of the 11th International Congress of Applied Mechanics, Ed. H. Gortler, Munich, Germany, pp. 973-979.
- Potter, J. L., Kinslow, M. and Boylan, D. E., 1966, "An Influence of the Orifice on Measured Pressures in Rarefied Flow", Rarefied Gas Dynamics, Ed. J. H. de Leeuw, Academic Press, New York, Vol. II, pp. 175-194.
- Santos, W. F. N., 2001, "Rarefied Hypersonic Flow Past the Sharp/Blunt Leading Edge of a Flat Plate", Proceedings of the 2nd International Conference on Computational Heat and Mass Transfer, Rio de Janeiro, RJ, Brazil.
- Santos, W. F. N., 2007, "The Underwedge-Surface Angle Effects on the Flowfield Structure of a Sharp Leading Edge in Hypersonic Flow", X Encontro de Modelagem Computacional, Nova Frigurgo, RJ.

8. RESPONSIBILITY NOTICE

The author is the only responsible for the printed material included in this paper.